Title

Statistical Analysis of Tri-Cresyl Phosphate Conversion on an Iron Oxide Surface Using Reactive Molecular Dynamics Simulations

Journal

The Journal of Physical Chemistry C, 123(20)

ISSN

1932-7447

Authors

Khajeh, Arash
Hu, Xiaoli
Mohammadtabar, Karen
et al.

Publication Date

2019-05-23

DOI

10.1021/acs.jpcc.9b02394

Peer reviewed

The Journal of Physical Chemistry C 2019 123 (20), 12886-12893
DOI: 10.1021/acs.jpcc.9b02394

Statistical Analysis of Tri-cresyl Phosphate Conversion on an Iron Oxide Surface Using Reactive Molecular Dynamics Simulations

Arash Khajeh,[†] Xiaoli Hu,[†] Karen Mohammadtabar,[†] Yun Kyung Shin,[‡] Adri C. T. van Duin,[‡] Stephen Berkebile,[¶] and Ashlie Martini[*,†]

†*Department of Mechanical Engineering, University of California Merced*

‡*Department of Mechanical and Nuclear Engineering, Pennsylvania State University*

¶*U.S. Army Research Laboratory*

E-mail: amartini@ucmerced.edu

Abstract

Parallel reactive molecular dynamics simulations were used to statistically analyze chemical reactions between tri-cresyl phosphate (TCP) and an amorphous iron oxide surface. To accurately model this system, a new parameter set for Fe/P/O interactions within the ReaxFF framework was developed. Using the new parameter set, 100 parallel simulations of a single TCP molecule on an amorphous iron oxide surface were run to capture multiple possible reactions at temperatures ranging from 300 to 700 K. The frequency of TCP–surface reactions for each atom type and each unique reaction site on the TCP was analyzed across the range of temperatures. Finally, the composition of the material chemisorbed to the surface was determined and compared to results from previously reported experimental measurements of TCP films in oxygen deficient environments. The results are specifically relevant to TCP, but the parallel reactive simulation approach and statistical analysis of reaction sites can be applied more generally to a range of chemical systems, particularly those involving complex molecules and disordered surfaces where many different reactions are possible.

Introduction

Many solid or semi-solid films are grown using techniques that involve gas or liquid phase species chemically reacting with a solid surface. Understanding the initial chemisorption reactions leading to film growth is an important step towards optimization of these films. Such reactions can be inferred from measured rates of film growth and surface characterization, but the elementary steps cannot readily be observed experimentally. An alternative to experimental approaches is atomistic modeling methods, i.e. density functional theory (DFT), kinetic Monte Carlo (KMC) or molecular dynamics simulation (MD), that provide atomic scale information about the elementary reaction steps. However, the challenge for simulation-based approaches is that film growth may occur through many different reactions

with varying statistical likelihood, especially at high temperatures or on irregular, e.g. amorphous or disordered, surfaces. DFT can provide detailed and highly accurate information about a given reaction, but the reactions must be identified *a priori* and the computational cost of the method typically means that only a few possible reactions can be studied (e.g.[1–3]). KMC enables much larger systems to be modeled, but the kinetics are typically based on DFT calculations so the approach is again limited to known reactions (e.g.[4–6]). In MD, multiple reactions can be identified during the simulation as atoms interact and move, but traditional MD is limited to relatively small size (nanometer) and time (nanosecond) scales, which means that only one or a few reactions will be identified (e.g.[7?,8]). Thus, standard atomistic approaches are not ideal tools for investigating film growth processes that involve many different possible reactions.

One way to simulate a larger number of different reactions is to extend the duration of MD simulations. This can be done using a variety of techniques,[9] including parallelization in time, i.e. multiple replicas of a model system run in parallel. It has been shown that parallelization does not have an effect on the relative probabilities of possible reactions, so both the sequence of reactions and reaction times in a parallel simulation are the same as those that would be observed in one long serial simulation.[10] For surface reactions that may be the precursors to film growth, use of multiple replicas enables statistical analysis of the possible reaction sites. To model chemical reactions on surfaces, these parallel simulations have been performed either using hybrid quantum mechanical/molecular dynamics methods[11,12] or molecular dynamics with reactive empirical potentials.[13–16] Such simulations have been applied to model SiH_3 on amorphous silicon,[14] oxynitridation on Si(001),[13] N adatoms on vanadium nitride (001),[11] oxidation of Si(100),[15] C_{60} molecules on a diamond substrate,[16] and Ar plasma bombardment on an organosilicate glass.[12] These studies demonstrate the utility of parallel reactive simulations for statistical analysis of reactions leading to film growth, and specifically surface reactivity. Here,

we study a more complex reactant molecule that contains multiple possible sites for chemisorption and so focus on the reactant as opposed to the surface.

The specific system investigated is tri-cresyl phosphate (TCP) interacting with an amorphous iron oxide surface. This system is highly relevant because TCP is a common aviation lubricant additive that functions by chemically reacting with ferrous surfaces to form protective films. Such films play a key role in enabling moving mechanical components to operate efficiently, but the elementary steps leading to film growth are still poorly understood. Experimental studies have been performed to characterize TCP films for several decades and have suggested multiple possible film formation mechanisms, including corrosion, thermal decomposition, hydrolytic decomposition, and oxidative decomposition.[17] However, few simulation-based studies have sought to explore these mechanisms. Non-reactive MD simulations of TCP and tri-n-butyl-phosphate have been reported,[18,19] but none included chemical reactions with iron oxide, in part due to lack of availability of an empirical potential for all of the necessary interactions. Also, the present authors used DFT to study three of the previously-proposed mechanisms for TCP on Fe(110) and found them all energetically feasible.[3] However, as mentioned previously, the limitations of DFT precluded a statistical analysis of reactions sites.

In this study, we applied parallel reactive MD simulations to model chemical reactions between TCP and an amorphous iron oxide surface. The simulations used the ReaxFF force field,[20] for which we developed new parameters to describe Fe/P/O interactions. Parameterization included Fe–O–P and Fe–P–O angles for a PO molecule on an iron(110) surface, Fe–P bond dissociation, Fe(II)–O–P and Fe(III)–O–P angle bending for gas phase species, and binding energies for P and PO on the bridge and hollow sites on an Fe(100) surface. The simulations described interactions between a single TCP molecule and the amorphous iron oxide surface at temperatures from 300 to 700 K. At each temperature, one hundred replica simulations were run, where the replicas differed only in the initial position of the TCP relative to the surface and the initial velocity distribution of the atoms. We analyzed

the frequency of TCP–surface reactions for each atom type and each unique reaction site on the TCP. Then, the composition of the chemisorbed material was analyzed and compared to previous experimental measurements. The results are relevant to TCP film growth specifically, but the approach demonstrated here can be applied more generally to study reaction sites on organic molecules using parallel reactive MD with statistical analysis.

Methods

Force field parameterization

Reactions between TCP and amorphous iron oxide were modeled using MD simulations with the ReaxFF force field.[20] Parameters for Fe/O/C/H interactions were taken from Ref.[21] (which used Fe/C parameters from[22]), and P/O/C/H interactions were taken from Ref.[23] However, to describe the Fe–P interactions, it was necessary to develop a new parameter set. This was done by training the force field to reproduce energies calculated using DFT. The parameterization included the following: Fe–O–P and Fe–P–O angles for a PO molecule on an iron(110) surface, Fe–P bond dissociation, Fe(II)–O–P and Fe(III)–O–P angle bending for gas phase species, and binding energies for P and PO on the bridge and hollow sites on an Fe(100) surface.

In the DFT calculations, the adsorption energy was obtained for P and PO species on a bcc Fe(001) slab consisting of six layers. The Fe(001) slab was generated by cleaving a periodic ($2 \times 2 \times 3$) supercell of bcc Fe along the (001) surface plane with a 2.0 nm vacuum space between the periodic Fe slabs. This slab model corresponds to a surface coverage of 0.25 ML when there is one adsorbate species on the surface. Adsorption was allowed on only one of the two surfaces. The spin-polarized first-principles DFT calculations were performed using the Vienna ab initio simulation package (VASP)[24] with plane wave basis sets. The DFT calculations used projector augmented wave (PAW)[25] pseudo-potentials and Perdew-Burke-Ernzerhof (PBE)[26] exchange-correlation functional with an energy cutoff of 550 eV. The Bril-

louin zone was sampled with a 5 × 5 × 1 Monkhorst-Pack[27] k-point mesh. The lattice parameters remained fixed to the Fe bulk lattice parameters in the ground state (a = 0.2834 nm) and ionic coordinates of atoms of top three layers were relaxed while the bottom three layers were fixed.

The valence angle potential energies for Fe-O-P bond angles in gaseous molecular species of iron(II) and iron(III) phosphate were calculated with Jaguar software package[28] using B3LYP method with the LACV3P+G* basis set. To obtain the potential energy profile along the valence angle distortion in a molecular fragment, the constrained geometry optimization was applied to Fe-O-P angle (75° ≤ A(Fe-O-P) ≤ 125°). The atomic coordinates of all atoms in the system were allowed to fully relax to obtain the optimized structure with a fixed valence angle.

Reactive molecular dynamics simulations

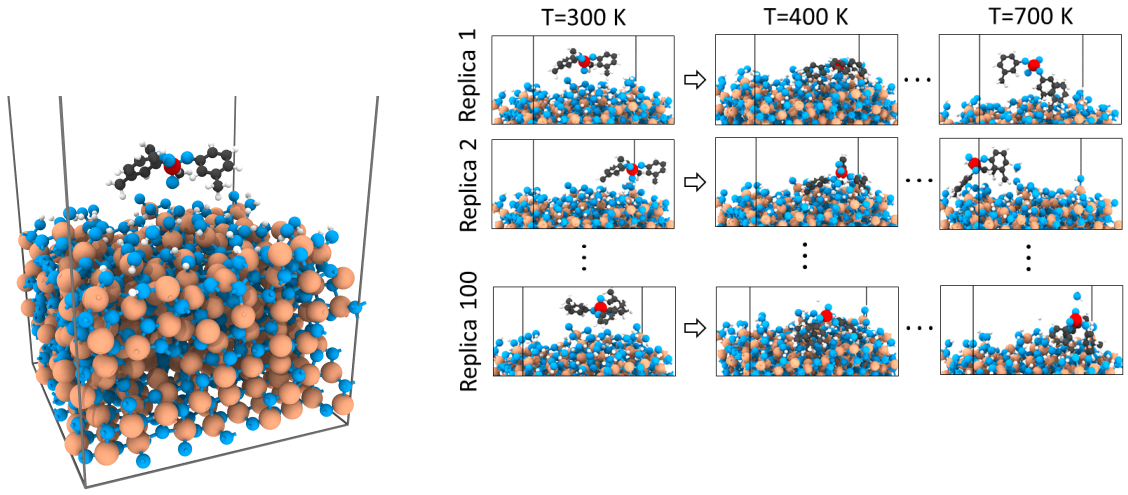

(a) (b)

Figure 1: (a) Snapshot of one model system consisting of a TCP molecule on a passivated amorphous iron oxide surface. (b) This model was replicated 100 times with different initial positions of the TCP relative to the surface and run at temperatures from 300 to 700 K. Red, black, blue, orange and white spheres represent phosphorus, carbon, oxygen, iron and hydrogen atoms, respectively.

The MD model system consisted of a single TCP molecule on an amorphous iron oxide surface. The amorphous iron oxide was created by first annealing a slab of crystalline Fe_3O_4 (2.5 nm × 2.5 nm in the plane of the surface and 2.0 nm

thick). The bottom 0.3 nm of the substrate was held fixed, forming the boundary in the surface-normal direction, and periodic boundary conditions were applied in the directions in the plane of the surface. Next, to create the amorphous material, the temperature was first increased from 300 to 4000 K over 25 ps, held at 4000 K for 125 ps, and then decreased back to 300 K over 500 ps. Prior to amorphization, the iron coordination number was 4 (37%) or 6 (63%), as expected based on the Fe_3O_4 crystal structure. After the amorphization process, the coordination number for most of the iron atoms was 4 (78% in the bulk and 80% on the surface), with the remaining atoms having coordination numbers of 1 (0.2% bulk, 3% surface), 2 (3% bulk, 8% surface), 3 (17% bulk and 8% surface) and 5 (1% bulk, 0% surface). Finally, to passivate the surface, 300 water molecules were placed over the amorphous iron oxide surface and the temperature of the system was set to 700 K for 500 ps to accelerate the hydroxylation reactions. The simulation was run until the potential energy was stable, after which any atoms not covalently bonded to the surface were removed. At the end of this process, the hydroxyl group density on the surface was 8.31 nm^{-2}, consistent with the range of 5 to 9 nm^{-2} reported in previous studies.[?]

This substrate was used to create 100 model systems with a single TCP molecule at different and randomly chosen initial positions relative to the surface in each model. Two different initial TCP orientations were modeled, with the double-bonded oxygen atom pointing down towards the surface in 50 simulations and the oxygen pointing up in the other 50 simulations. A snapshot of one model system is shown in Fig. 1a. For all 100 models, MD simulations were run with the temperature controlled using a Nosé-Hoover thermostat applied to the free atoms. Simulations were run at 300–700 K in increments of 100 K for up to 1 ns, where the duration at each temperature was determined based on when the number of bonds reached steady state. At each temperature above 300 K, the initial configuration was taken from the final configuration of the simulation at the next lower temperature. Fig. 1b shows a schematic of the parallel simulation approach. Chemical bonding information was output at 1.25 ps intervals and a bond-order cut-off value of 0.3 was

used to identify covalent bonds. The number of bonds was averaged over the steady state region of the simulation (during the last 25 ps at each temperature).

All simulations were run using the large-scale atomic/molecular massively parallel simulator (LAMMPS)[29] with a timestep of 0.25 fs, and post processing of results was carried out using OVITO software.[30]

Results and Discussion

Comparisons between energies obtained from ReaxFF with the new parameter set and DFT are reported in Table 1 and Fig. 2. For the binding energies in Table 1, reasonable agreement between DFT and ReaxFF was observed, with less than 1 kcal/mol difference for the P binding energies and less than 8 kcal/mol difference for the PO binding energies. Further, the relative energies of the hole and bridge sites were captured by ReaxFF. Bond and angle energies are shown in Fig. 2, where snapshots of the model systems are provided in the insets. ReaxFF energies agreed with DFT, particularly near the equilibrium distances and angles. In some cases, far from equilibrium, the energy trend predicted by the force field deviated from the DFT results (e.g. Fig. 2a above 120°). However, these deviations were only observed for energetically unfavorable configurations with high angle strain, which were given relatively low priority in the training process. Importantly, for the highly relevant bond distances and valence angles near equilibrium, ReaxFF captures the DFT data well. The final parameter set is given in the Supplemental Information.

Table 1: Comparison of binding energies calculated with DFT and ReaxFF.

System	Binding energies (kcal/mol)	
	DFT	ReaxFF
P bridge	-92.41	-92.12
P hole	-128.22	-128.85
PO bridge	-63.79	-71.95
PO hole	-89.81	-85.74

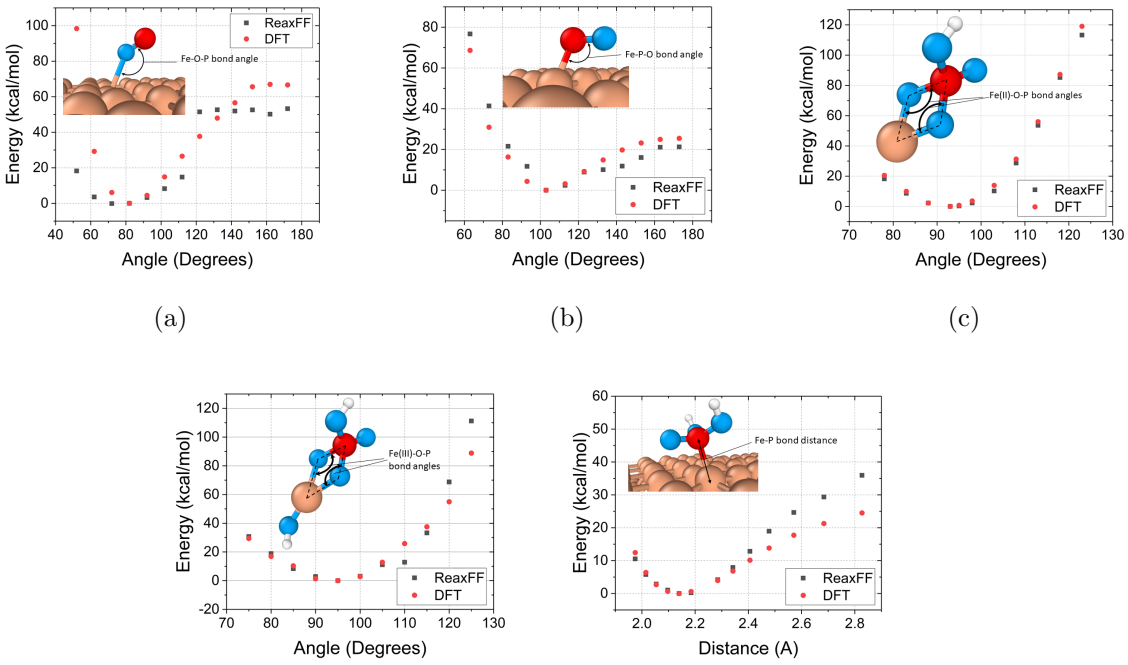

Figure 2: Comparison of bond and angle energies calculated using ReaxFF and DFT: (a) Valence angle energies for the Fe–O–P angle; (b) Valence angle energies for the Fe–P–O angle; (c) Fe(II)–O–P angle energies; (d) Fe(III)–O–P angle energies; (e) Fe–P bond dissociation energies.

Using this new parameter set, 100 parallel simulations of TCP on an amorphous iron oxide surface were run. The number of covalent bonds formed between TCP and the surface was analyzed and categorized based on atom–atom type, i.e. Fe–C, Fe–O or O–P, where the first element corresponds to an atom in the iron oxide and the second is in the TCP. Bonds between all other combinations of atoms had a probability of less than 3% at any temperature, so they were not included in the analysis. Also, bonds with H atoms were excluded from the analysis since they do not contribute significantly to film formation. The probability of each bond at the different temperatures is shown in Fig. 3. Note that there was no difference between the trends exhibited by the simulations with the two different initial TCP orientations at 300K, so they were analyzed together. On average, there was more TCP–surface bonding at the higher temperatures, although the distribution of ele-

ments involved changed with temperature. Comparing the different types of bonds, it is evident that Fe–C bonds were the most common at any temperature.

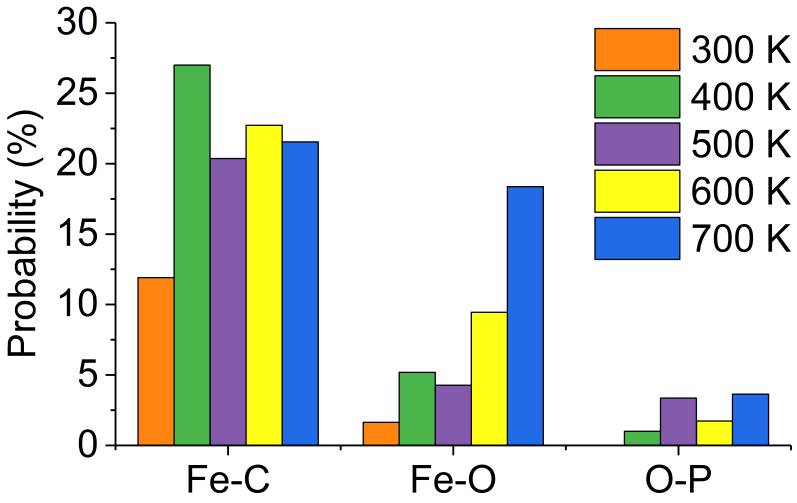

Figure 3: The probability of a bond forming between the TCP and amorphous iron oxide surface as a function of temperature for each atom–atom pair, where the first element corresponds to an atom in the iron oxide and the second is in the TCP.

The above analysis considers the Fe–C bonds and the Fe–O bonds collectively. However, in reality there are seven unique C atoms and two unique O atoms available for reaction on the TCP, in addition to the P atom. The unique reaction sites on the TCP are identified and labeled in the upper left panel of Fig. 4. The probability analysis was then repeated for each unique reaction site on the TCP and the results are illustrated graphically in Fig. 4. At temperatures between 300 and 500 K, the most reactive atoms were C5 and C6, likely because of their location at the outermost edge of the benzene ring. As the temperature increased, the O atoms became more reactive, until O1 was the most reactive site on the TCP at 700 K. At the highest temperatures, we also observed statistically significant reactions at the C1 and C7 sites.

To quantify the above analysis, we calculated the probability of bonding for each possible combination of a unique reaction site on the TCP molecule and a surface atom. The result is reported in Fig. 5, where only reactions with a probability above 3% at any temperature are shown. The statistically significant reaction pairs were

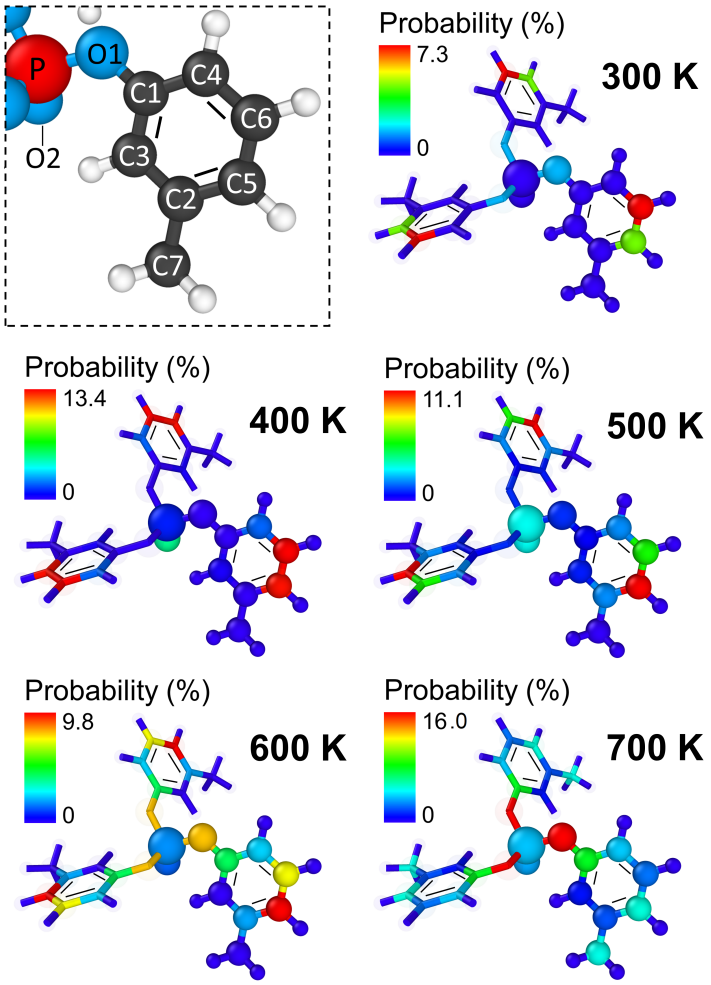

Figure 4: The reactivity of individual atoms in the TCP molecule at different temperatures. The unique reaction sites on the TCP are identified and labeled in the upper left panel. Note that the ranges of the color scales are different for each temperature, so this figure does not enable comparison between temperatures but rather comparison between the different reaction sites at each temperature.

Fe–C1, Fe–C4, Fe–C5, Fe–C6, Fe–C7, Fe–O1, Fe–O2 and O–P. Again, bonds with H atoms were excluded from the analysis. Snapshots of representative model systems illustrating the statistically significant reactions are shown in Fig. 6. Fig. 5 confirms that most probable reactions at lower temperatures involved chemical bonding between the C5 or C6 atom in the TCP and Fe on the iron oxide surface. These reactions were observed for whole TCP molecules, i.e. without decomposition. However, at the high temperatures, reactions between O1 and C1 in the TCP and Fe on the surface became dominant. At these temperatures, chemisorption reactions were accompanied by TCP decomposition. The most commonly observed reaction at high

temperatures was decomposition of TCP via breaking of the O1–C1 bond followed by chemisorption of cresyl via an O1–Fe bond. This was also sometimes followed by C1–Fe bonding, explaining the consistent trends exhibited by O1–Fe and C1–Fe observed in Fig. 5.

Previous DFT studies analyzed reaction pathways for TCP on an iron (110) surface and showed that multiple pathways were possible.[3] However, all of those pathways started with bonding between O2 and Fe. The dynamic simulations shown here suggest that, while Fe–O2 bonding can occur on an amorphous iron oxide surface, it is not statistically significant compared to Fe–C or Fe–O1. This highlights the differences between reactions on ideal crystalline metal surfaces compared to those on an amorphous, passivated oxide.

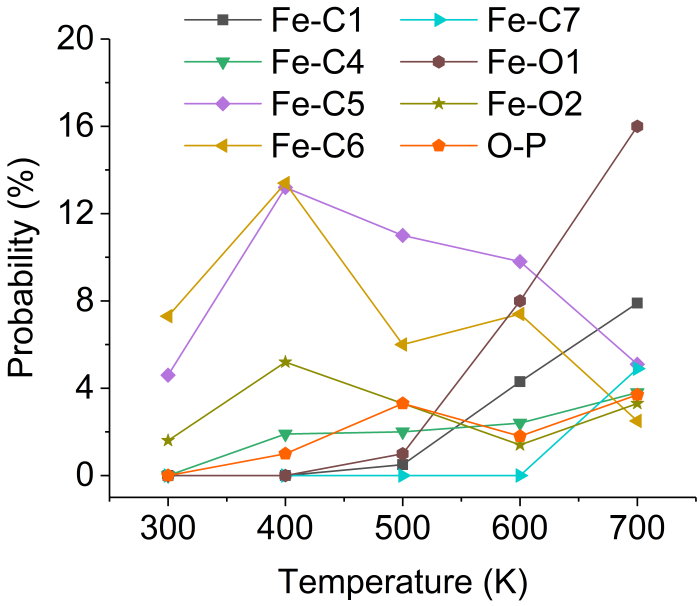

Figure 5: Probability of bonding between unique reaction sites on the TCP and atoms on the iron oxide surface as a function of temperature. Only atom–atom pairs for which the probability of bonding was 3% or more at any temperature are shown.

The chemical reactions described above are the starting point for film formation. Therefore, the composition of the material chemisorbed to the surface in the simulations can be analyzed in the context of previous experimental measurements; specifically, experiments performed in oxygen-deficient environments, where the iron

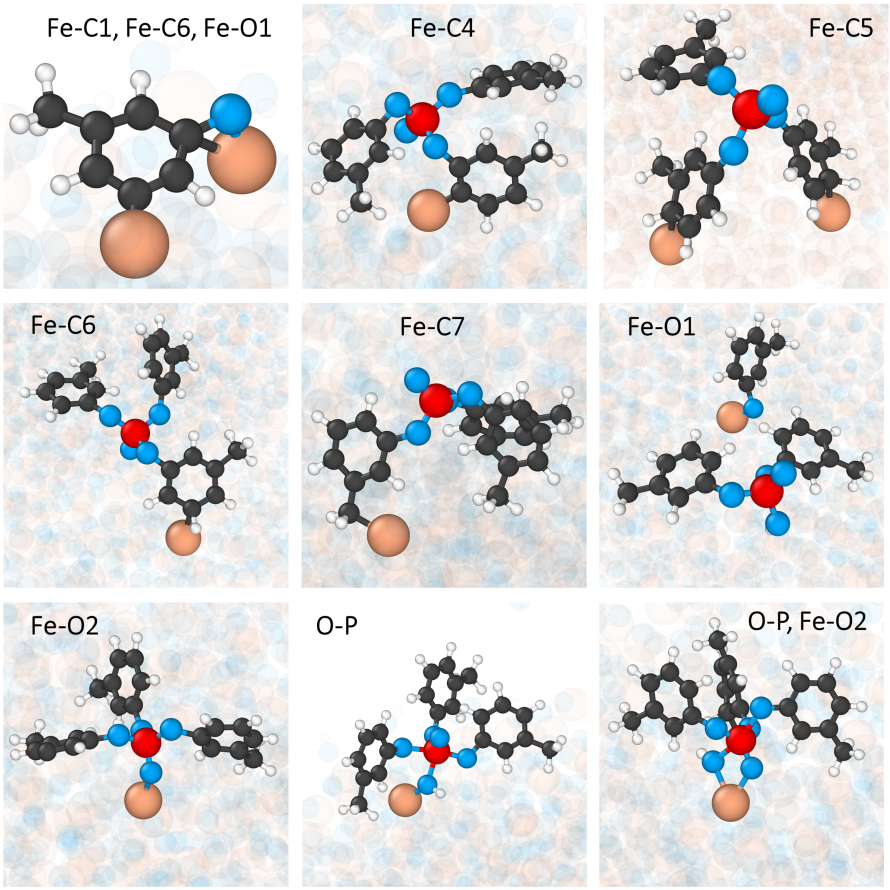

Figure 6: Snapshots of the simulation illustrating the statistically significant TCP–surface interactions. All atoms are faded except those in the TCP and surface involved in a given reaction.

was expected to have a native oxide, but only small amounts of outside reactants (e.g. water, oxygen, hydrogen) were available to contribute to the TCP-surface reactions.[31–34] In the simulations, the composition of the material chemisorbed to the surface was quantified in terms of surface density of individual elements that originated from TCP molecules. Figure 7 shows that the chemisorbed material consisted of C, O and P atoms. The density of the individual elements was greatest at 400 K and, at all temperatures, C had the highest density.

Although direct comparisons between simulations and experiments cannot be made since the models capture just the initial stage of film formation, parallels can be drawn between the composition of chemisorbed species in these simulations and the composition of TCP films measured in previous oxygen-deficient experimental studies. First, the significant amount of C observed in the simulations is consistent

with experimental measurements of the composition of TCP films near the surface obtained using auger electron spectroscopy (AES) and x-ray photoelectron spectroscopy (XPS).[31,32] Further, analysis of the species chemisorbed to the surface in the simulations showed that, at lower temperatures, most chemisorbed species were complete TCP molecules, but as the temperature increased, bonds broke within the TCP resulting in chemisorption of decomposition products, predominantly cresyl. This is consistent with the composition of reactant films obtained using Auger Electron Spectroscopy (AES) and X-ray Photoelectron Spectroscopy (XPS) on the surface of iron foils exposed to TCP at elevated temperatures in an oxygen-starved environment.[31–33] Our simulations suggest both occur, with the statistical likelihood of the latter increasing with temperature.

Most previous experimental studies have identified phosphorous as a key component of films formed from TCP on ferrous surfaces[17] and the working assumption has been that this iron phosphide or iron phosphate film results from the formation of Fe–P bonds directly from the TCP molecule.[3] However, our results show that P atoms are more often indirectly bonded[35] to the surface through TCP or other species that bond with the surface via C atoms. Also, phosphate groups are likely to be present on the surface through physisorption, following chemisorption of cresyl. Therefore, at least in oxygen deficient environments, the primary mechanisms by which P is initially incorporated into a film are indirect bonding (i.e. present in species bonded to the surface via other atoms) or physisorption enabled by decomposition of TCP. This hypothesis cannot be directly tested without further extensive experimentation and reactive MD simulations. However, many previous experiments analyzed TCP film formation in terms of the composition of desorbed species, as opposed to adsorbed species as done here. Therefore, future research specifically analyzing reaction products that leave the surface would enable additional comparisons to experiment.

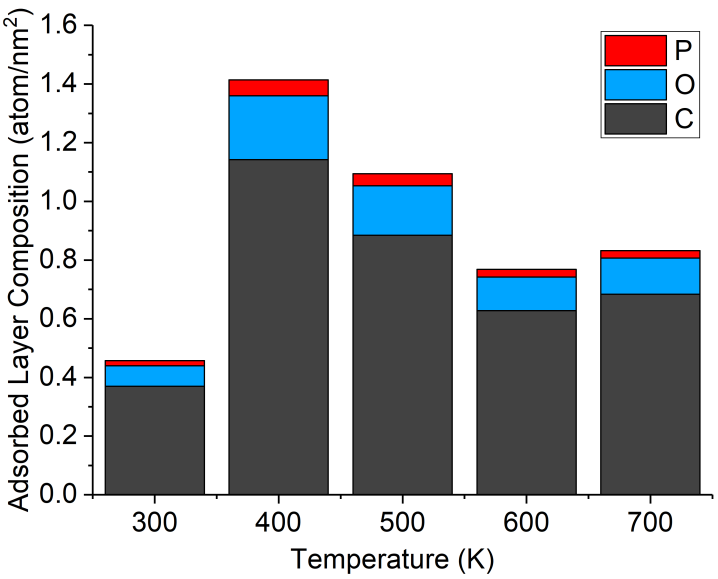

Figure 7: Chemical composition of adsorbed layer on the amorphous iron oxide surface at different temperatures.

Conclusion

This study used parallel reactive molecular dynamics simulations of TCP on an amorphous iron oxide surface to explore the initial steps leading to formation of a protective film on lubricated ferrous surfaces. To enable these simulations, a new parameter set for ReaxFF was developed to capture Fe/P/O interactions. Many reaction pathways are possible for TCP on iron oxide because of the multiple reaction sites on the TCP and irregularity of the amorphous surface. To capture as many of these pathways as possible in an MD simulation, we ran 100 parallel replicas of a model system consisting of one TCP at random initial locations above the surface. The simulations were run at temperatures ranging from 300 to 700 K and results were analyzed at each temperature to determine the statistical likelihood of the possible reactions. It was found that the relative reactivity of the unique reaction sites on the TCP was temperature dependent. Specifically, C atoms at the perimeter of the rings bonded most with the surface at lower temperatures and O atoms in the core of the TCP bonded most with the surface at higher temperatures. The composition of the material chemisorbed to the surface was then analyzed which

revealed that C is the most prevalent element at any temperature. Also, the most statistically likely chemisorbed species were found to be TCP or cresyl, with the former being more prevalent at lower temperatures and the latter more prevalent at higher temperatures. These trends were found to be consistent with observations from previous experimental measurements of TCP films grown on iron with a native oxide in oxygen-deficient environments.

Overall, this study has three key outcomes. First, a parameter set was developed for Fe/P/O interactions by tuning parameters to capture interactions and reactions between TCP and an iron oxide surface. This parameter set may be used for ReaxFF simulations of other model systems containing Fe, P and O, but the force field should be tested to ensure transferability. To enable the force field to be used more generally, parameterization could be extended in future studies to include Fe–P crystal phases, as well as reaction pathways for TCP on crystalline iron surfaces.[3] Second, the findings illustrate that there are multiple reactions between TCP and an amorphous iron oxide, and the statistical likelihood of these reactions will depend on temperature. Further, simulations results suggest that the presence of phosphorous in films formed from TCP may be due to molecules that bond with the surface via carbon. Third, the statistical approach used to characterize reaction sites on TCP as it interacts and bonds with amorphous iron oxide may be applied to other systems where organic molecules react with surfaces. The approach is particularly useful for irregular or disordered surfaces which are present in a variety of applications and on which many possible reactions contribute to film formation.

Supporting Information

ReaxFF force field parameters for C/H/O/Fe/P with new parameterization for: Fe–O–P and Fe–P–O angles for a PO molecule on an iron(110) surface, Fe–P bond dissociation, Fe(II)–O–P and Fe(III)–O–P angle bending for gas phase species, and binding energies for P and PO on the bridge and hollow sites on an Fe(100) surface.

Acknowledgements

This research was sponsored by the Army Research Laboratory and was accomplished under Cooperative Agreement Number W911NF-16-2-0121. The views and conclusions contained in this document are those of the authors and should not be interpreted as representing the official policies, either expressed or implied, of the Army Research Laboratory or the US Government. The US Government is authorized to reproduce and distribute reprints for Government purposes notwithstanding any copyright notation herein. We also greatly appreciate the assistance of Dr. Jejoon Yeon for instruction and guidance on training the ReaxFF force field parameters and Dr. Eric Osei-Agyemang for performing preliminary DFT calculations.

References

(1) Onodera, T.; Kawasaki, K.; Nakakawaji, T.; Higuchi, Y.; Ozawa, N.; Kurihara, K.; Kubo, M. Effect of tribochemical reaction on transfer-film formation by poly (tetrafluoroethylene). *J. Phys. Chem. C* **2014**, *118*, 11820–11826.

(2) Kokalj, A.; Peljhan, S. Density functional theory study of ATA, BTAH, and BTAOH as copper corrosion inhibitors: adsorption onto Cu (111) from gas phase. *Langmuir* **2010**, *26*, 14582–14593.

(3) Osei-Agyemang, E.; Berkebile, S.; Martini, A. Decomposition mechanisms of anti-wear lubricant additive tricresyl phosphate on iron surfaces using DFT and atomistic thermodynamic studies. *Tribol. Lett.* **2018**, *66*, 48.

(4) Cuppen, H. M.; Karssemeijer, L. J.; Lamberts, T. The kinetic Monte Carlo method as a way to solve the master equation for interstellar grain chemistry. *Chem. Rev.* **2013**, *113*, 8840–8871.

(5) Mei, D.; Sheth, P. A.; Neurock, M.; Smith, C. M. First-principles-based kinetic Monte Carlo simulation of the selective hydrogenation of acetylene over Pd (111). *J. Catal.* **2006**, *242*, 1–15.

(6) Eckert, M.; Neyts, E.; Bogaerts, A. Insights into the growth of (ultra) nanocrystalline diamond by combined molecular dynamics and Monte Carlo simulations. *Cryst. Growth & Des.* **2010**, *10*, 3005–3021.

(7) Khajeh, A.; He, X.; Yeon, J.; Kim, S. H.; Martini, A. Mechanochemical association reaction of interfacial molecules driven by shear. *Langmuir* **2018**, *34*, 5971–5977.

(8) Yue, D.-C.; Ma, T.-B.; Hu, Y.-Z.; Yeon, J.; van Duin, A. C. T.; Wang, H.; Luo, J. Tribochemistry of phosphoric acid sheared between quartz surfaces: A reactive molecular dynamics study. *J. Phys. Chem. C* **2013**, *117*, 25604–25614.

(9) Voter, A. F.; Montalenti, F.; Germann, T. C. Extending the time scale in atomistic simulation of materials. *Annu. Rev. Mater. Res.* **2002**, *32*, 321–346.

(10) Perez, D.; Uberuaga, B. P.; Voter, A. F. The parallel replica dynamics method – Coming of age. *Comp. Mat. Sci.* **2015**, *100*, 90–103.

(11) Sangiovanni, D. G.; Mei, A. B.; Hultman, L.; Chirita, V.; Petrov, I.; Greene, J. E. Ab initio molecular dynamics simulations of nitrogen/VN (001) surface reactions: Vacancy-catalyzed N_2 dissociative chemisorption, N adatom migration, and N_2 desorption. *J. Phys. Chem. C* **2016**, *120*, 12503–12516.

(12) Rimsza, J. M.; Du, J. Surface reactions and structural evolution of organosilicate glass under Ar plasma bombardment. *Comp. Mater. Sci.* **2015**, *110*, 287–294.

(13) Cao, H.; Srivastava, P.; Choi, K.; Kim, S.; Lee, K.-R. Early stage oxynitridation process of Si (001) surface by NO gas: Reactive molecular dynamics simulation study. *J. Appl. Phys.* **2016**, *119*, 125305.

(14) Valipa, M. S.; Sriraman, S.; Aydil, E. S.; Maroudas, D. Atomic-scale analysis of fundamental mechanisms of surface valley filling during plasma deposition of amorphous silicon thin films. *Surf. Sci.* **2005**, *574*, 123–143.

(15) Pamungkas, M. A.; Joe, M.; Kim, B.-H.; Lee, K.-R. Reactive molecular dynamics simulation of early stage of dry oxidation of Si (100) surface. *J. Appl. Phys.* **2011**, *110*, 053513.

(16) Chang, J.-G.; Hwang, C.-C.; Ju, S.-P.; Huang, S.-H. A molecular dynamics simulation investigation into the structure of fullerene C60 grown on a diamond substrate. *Carbon* **2004**, *42*, 2609–2616.

(17) Guan, B.; Pochopien, B. A.; Wright, D. S. The chemistry, mechanism and function of tricresyl phosphate (TCP) as an anti-wear lubricant additive. *Lubr. Sci.* **2016**, *28*, 257–265.

(18) Irving, D. L.; Brenner, D. W. Diffusion on a self-assembled monolayer: molecular modeling of a bound + mobile lubricant. *J. Phys. Chem. B* **2006**, *110*, 15426–15431.

(19) Cui, S.; de Almeida, V. F.; Hay, B. P.; Ye, X.; Khomami, B. Molecular dynamics simulation of tri-n-butyl-phosphate liquid: A force field comparative study. *J. Phys. Chem. B* **2012**, *116*, 305—-313.

(20) van Duin, A. C. T.; Dasgupta, S.; Lorant, F.; Goddard, W. A. ReaxFF: A reactive force field for hydrocarbons. *Phys. Chem. A* **2001**, *105*, 9396–9409.

(21) Shin, Y. K.; Kwak, H.; Vasenkov, A. V.; Sengupta, D.; van Duin, A. C. T. Development of a reaxFF reactive force field for Fe/Cr/O/S and application to oxidation of butane over a pyrite-covered Cr_2O_3 catalyst. *ACS Catal.* **2015**, *5*, 7226–7236.

(22) Zou, C.; van Duin, A.; Sorescu, D. Theoretical investigation of hydrogen adsorption and dissociation on iron and iron carbide surface using the ReaxFF reactive force field method. *Top. Catal.* **2012**, *55*, 391–401.

(23) Verlackt, C. C. W.; Neyts, E. C.; Jacob, T.; Fantauzzi, D.; Golkaram, M.; Shin, Y.; van Duin, A.; Bogaerts, A. Atomic-scale insight into the interactions

between hydroxyl radicals and DNA in solution using the ReaxFF reactive force field. *New J. Phys.* **2015**, *15*, 103005.

(24) Kresse, G.; Furthmüller, J. Efficient iterative schemes for ab initio total-energy calculations using a plane-wave basis set. *Phys. Rev. B* **1996**, *54*, 11169–11186.

(25) Blöchl, P. E. Projector augmented-wave method. *Phys. Rev. B* **1994**, *50*, 17953–17979.

(26) Perdew, J. P.; Burke, K.; Ernzerhof, M. Generalized gradient approximation made simple. *Phys. Rev. Lett.* **1996**, *77*, 3865–3868.

(27) Monkhorst, H. J.; Pack, J. D. Special points for Brillouin-zone integrations. *Phys. Rev. B* **1976**, *13*, 5188–5192.

(28) Bochevarov, A. D.; Harder, E.; Hughes, T. F.; Greenwood, J. R.; Braden, D. A.; Philipp, D. M.; Rinaldo, D.; Halls, M. D.; Zhang, J.; Friesner, R. A. Jaguar: a high-performance quantum chemistry software program with strengths in life and materials sciences. *Int. J. Quantum Chem.* **2013**, *113*, 2110–2142.

(29) Plimpton, S. Fast parallel algorithms for short-range molecular dynamics. *J. Comp. Phys.* **1995**, *117*, 1–19.

(30) Stukowski, A. Visualization and analysis of atomistic simulation data with OVITO – the Open Visualization Tool. *Model. Simul. Mater. Sc.* **2009**, *18*, 015012.

(31) Johnson, D. W.; Morrow, S.; Forster, N. H.; Saba, C. S. Vaporphase lubrication: reaction of phosphate ester vapors with iron and steel. *Chem. Mater.* **2002**, *14*, 3767—-3775.

(32) Johnson, D. W.; Hils, J. E. Phosphate esters, thiophosphate esters and metal thiophosphates as lubricant additives. *Lubricants* **2013**, *1*, 132—-148.

(33) Saba, C. S.; Forster, N. H. Reactions of aromatic phosphate esters with metals and their oxides. *Tribol. Lett.* **2002**, *12*, 135—146.

(34) Pavelko, G. F. The mechanism of iron phosphide formation during boundary friction in the presence of organic phosphates and phosphites. *Wear* **2012**, *33*, 115—123.

(35) Khajeh, A.; Krim, J.; Martini, A. Synergistic effect of nanodiamonds on the adsorption of tricresyl phosphate on iron oxide surfaces. *Appl. Phys. Lett.* **2019**, *114*, 171602.

Supplemental Information

Reactive MD-Force Field: C/H/O/Fe/P ReaxFF Force Field of P on Fe Surface 2019

39 ! Number of general parameters

50.0000 !Overcoordination parameter

9.5469 !Overcoordination parameter

26.5405 !Valency angle conjugation parameter

1.7224 !Triple bond stabilisation parameter

6.8702 !Triple bond stabilisation parameter

60.4850 !C2-correction

1.0588 !Undercoordination parameter

4.6000 !Triple bond stabilisation parameter

12.1176 !Undercoordination parameter

13.3056 !Undercoordination parameter

-70.5044 !Triple bond stabilization energy

0.0000 !Lower Taper-radius

10.0000 !Upper Taper-radius

2.8793 !Not used

33.8667 !Valency undercoordination

6.0891 !Valency angle/lone pair parameter

1.0563 !Valency angle

2.0384 !Valency angle parameter

6.1431 !Not used

6.9290 !Double bond/angle parameter

0.3989 !Double bond/angle parameter: overcoord

3.9954 !Double bond/angle parameter: overcoord

-2.4837 !Not used

5.7796 !Torsion/BO parameter

10.0000 !Torsion overcoordination

1.9487 !Torsion overcoordination

-1.2327 !Conjugation 0 (not used)

2.1645 !Conjugation

1.5591 !vdWaals shielding

0.1000 !Cutoff for bond order (*100)

2.1365 !Valency angle conjugation parameter

0.6991 !Overcoordination parameter

50.0000 !Overcoordination parameter

1.8512 !Valency/lone pair parameter

0.5000 !Not used

20.0000 !Not used

5.0000 !Molecular energy (not used)

0.0000 !Molecular energy (not used)

2.6962 !Valency angle conjugation parameter

5 ! Nr of atoms; cov.r; valency;a.m;Rvdw;Evdw;gammaEEM;cov.r2; alfa;gammavdW;valency;Eunder;Eov

cov r3;Elp;Heat inc.;n.u.;n.u.;n.u.;n.u.

ov/un;val1;n.u.;val3,vval4

C 1.3817 4.0000 12.0000 1.8903 0.1838 0.9000 1.1341 4.0000 9.7559

2.1346 4.0000 34.9350 79.5548 5.9666 7.0000 0.0000 1.2114 0.0000 202.5551

8.9539 34.9289 13.5366 0.8563 0.0000 -2.8983 2.5000 1.0564 4.0000 2.9663

0.0000 0.0000 0.0000

H 0.8930 1.0000 1.0080 1.3550 0.0930 0.8203 -0.1000 1.0000 8.2230 33.2894

1.0000 0.0000 121.1250 3.7248 9.6093 1.0000

-0.1000 0.0000 61.6606 3.0408 2.4197 0.0003 1.0698 0.0000

-19.4571 4.2733 1.0338 1.0000 2.8793 0.0000 0.0000 0.0000

O 1.2450 2.0000 15.9990 2.3890 0.1000 1.0898 1.0548 6.0000

9.7300 13.8449 4.0000 37.5000 116.0768 8.5000 8.3122 2.0000

0.9049 0.4056 59.0626 3.5027 0.7640 0.0021 0.9745 0.0000

-3.5500 2.9000 1.0493 4.0000 2.9225 0.0000 0.0000 0.0000

Fe 1.9029 3.0000 55.8450 2.0990 0.1181 0.4744 -1.6836 3.0000

10.8548 2.6084 3.0000 0.0000 18.3725 1.7785 8.6281 0.0000

-1.2000 0.0000 102.1000 25.3430 10.1260 0.7590 0.8563 0.0000

-16.0573 2.6997 1.0338 6.0000 2.5791 0.0000 0.0000 0.0000

P 1.5994 3.0000 30.9738 1.7000 0.1743 1.0000 1.3000 5.0000

9.1909 14.2932 5.0000 0.0000 0.0000 1.8292 7.2520 0.0000

-1.0000 10.2596 1.5000 0.2205 16.7429 15.9629 0.0000 0.0000

-2.5000 1.6114 1.0338 5.0000 2.8793 0.0000 0.0000 0.0000

15 ! Nr of bonds; Edis1;LPpen;n.u.;pbe1;pbo5;13corr;pbo6 pbe2;pbo3;pbo4;n.u.;pbo1;pbo2;ovcorr

1 1 158.2004 99.1897 78.0000 -0.7738 -0.4550 1.0000 37.6117 0.4147

0.4590 -0.1000 9.1628 1.0000 -0.0777 6.7268 1.0000 0.0000

1 2 169.4760 0.0000 0.0000 -0.6083 0.0000 1.0000 6.0000 0.7652

5.2290 1.0000 0.0000 1.0000 -0.0500 6.9136 0.0000 0.0000

2 2 153.3934 0.0000 0.0000 -0.4600 0.0000 1.0000 6.0000 0.7300

6.2500 1.0000 0.0000 1.0000 -0.0790 6.0552 0.0000 0.0000

1 3 164.4303 82.6772 60.8077 -0.3739 -0.2351 1.0000 10.5036 1.0000

0.4475 -0.2288 7.0250 1.0000 -0.1363 4.8734 0.0000 0.0000

2 3 160.0000 0.0000 0.0000 -0.5725 0.0000 1.0000 6.0000 0.5626

1.1150 1.0000 0.0000 0.0000 -0.0920 4.2790 0.0000 0.0000

3 3 142.2858 145.0000 50.8293 0.2506 -0.1000 1.0000 29.7503 0.6051

0.3451 -0.1055 9.0000 1.0000 -0.1225 5.5000 1.0000 0.0000

1 4 109.5214 0.0000 0.0000 0.6663 -0.3000 1.0000 36.0000 0.0100

1.0648 -0.3500 15.0000 1.0000 -0.1512 4.1708 1.0000 0.0000

2 4 78.2669 0.0000 0.0000 0.4668 0.0000 1.0000 6.0000 0.1766

0.5673 1.0000 0.0000 1.0000 -0.1543 5.4965 0.0000 0.0000

3 4 67.5128 0.0000 0.0000 0.1301 -0.3000 0.0000 36.0000 0.0852

1.0000 -0.3500 15.0000 1.0000 -0.0629 7.1208 0.0000 0.0000

4 4 41.4611 0.0000 0.0000 0.2931 -0.2000 0.0000 16.0000 0.2682

0.6294 -0.2000 15.0000 1.0000 -0.0512 6.8013 0.0000 0.0000

1 5 110.0000 92.0000 0.0000 0.2171 -0.1418 1.0000 13.1260 0.6000

0.3601 -0.1310 10.7257 1.0000 -0.0869 5.3302 1.0000 0.0000

2 5 0.1466 0.0000 0.0000 0.2250 -0.1418 1.0000 13.1260 0.6000

0.3912 -0.1310 0.0000 1.0000 -0.1029 9.3302 0.0000 0.0000

3 5 202.5868 164.1808 0.0000 0.5506 -0.5000 1.0000 25.0000 0.4300

0.0912 -0.1285 16.0342 1.0000 -0.2008 6.2678 1.0000 0.0000

4 5 267.6410 0.0000 0.0000 -0.9090 -0.3000 0.0000 36.0000 0.1000

1.7768 -0.3500 15.0000 1.0000 -0.0992 5.7752 0.0000 0.0000

5 5 0.0000 0.0000 0.0000 0.2171 -0.5000 1.0000 35.0000 0.6000

0.5000 -0.5000 20.0000 1.0000 -0.2000 10.0000 1.0000 0.0000

8 ! Nr of off-diagonal terms; Ediss;Ro;gamma;rsigma;rpi;rpi2

1 2 0.1239 1.4004 9.8467 1.1210 -1.0000 -1.0000

1 3 0.1345 1.8422 9.7725 1.2835 1.1576 1.0637

2 3 0.0283 1.2885 10.9190 0.9215 -1.0000 -1.0000

1 4 0.4204 1.4900 11.0144 1.4071 -1.0000 -1.0000

2 4 0.0200 1.9451 10.8595 1.4157 -1.0000 -1.0000

3 4 0.1000 1.8000 9.1989 1.7050 -1.0000 -1.0000

3 5 0.0611 1.7624 10.2685 1.7989 1.4523 -1.0000

4 5 0.2619 2.1638 11.2236 1.8799 -1.0000 -1.0000

52 ! Nr of angles;at1;at2;at3;Thetao,o;ka;kb;pv1;pv2

1 1 1 59.0573 30.7029 0.7606 0.0000 0.7180 6.2933 1.1244

1 1 2 65.7758 14.5234 6.2481 0.0000 0.5665 0.0000 1.6255

2 1 2 70.2607 25.2202 3.7312 0.0000 0.0050 0.0000 2.7500

1 2 1 0.0000 3.4110 7.7350 0.0000 0.0000 0.0000 1.0400 1 2 2 0.0000

0.0000 6.0000 0.0000 0.0000 0.0000 1.0400

2 2 2 0.0000 27.9213 5.8635 0.0000 0.0000 0.0000 1.0400

1 1 3 53.9517 7.8968 2.6122 0.0000 3.0000 58.6562 1.0338

3 1 3 76.9627 44.2852 2.4177 -25.3063 1.6334 -50.0000 2.7392

1 3 1 72.6199 42.5510 0.7205 0.0000 2.9294 0.0000 1.3096

1 3 3 81.9029 32.2258 1.7397 0.0000 0.9888 68.1072 1.7777

3 3 3 80.7324 30.4554 0.9953 0.0000 3.0000 50.0000 1.0783

2 1 3 65.0000 16.3141 5.2730 0.0000 0.4448 0.0000 1.4077

1 3 2 70.1101 13.1217 4.4734 0.0000 0.8433 0.0000 3.0000

2 3 3 75.6935 50.0000 2.0000 0.0000 1.0000 0.0000 1.1680

2 3 2 85.8000 9.8453 2.2720 0.0000 2.8635 0.0000 1.5800

1 2 3 0.0000 25.0000 3.0000 0.0000 1.0000 0.0000 1.0400

2 2 3 0.0000 8.5744 3.0000 0.0000 0.0000 0.0000 1.0421

3 2 3 0.0000 15.0000 2.8900 0.0000 0.0000 0.0000 2.8774

1 4 1 0.1000 42.2980 0.3169 0.0000 1.1069 0.0000 2.3466

1 1 4 74.8790 30.0000 2.0000 0.0000 2.0334 0.0000 1.0928

1 4 4 47.9341 1.0246 7.9341 0.0000 2.8853 0.0000 1.0000

4 1 4 33.2812 34.6443 3.0111 0.0000 0.1701 0.0000 1.0510

2 4 2 20.3683 0.0100 2.2825 0.0000 0.7660 0.0000 1.3788

2 2 4 0.0000 0.0100 1.0568 0.0000 1.8595 0.0000 3.6142

4 2 4 0.0000 10.4428 7.9607 0.0000 2.3717 0.0000 1.1970

2 4 4 48.4128 4.0632 0.6773 0.0000 2.2274 0.0000 1.8605

2 1 4 2.6539 32.1638 0.9167 0.0000 0.0240 0.0000 1.1158

1 4 2 42.7140 0.1451 0.2500 0.0000 0.0851 0.0000 2.8955

1 2 4 0.0000 0.0100 2.2066 0.0000 1.9789 0.0000 1.4466

1 3 4 90.0000 42.4716 6.6776 0.0000 2.4560 0.0000 1.6221

3 1 4 54.6900 12.6123 2.3543 0.0000 2.0000 0.0000 1.2513

1 4 3 38.2755 19.3103 0.1151 0.0000 0.7569 0.0000 2.3113

2 3 4 26.0012 49.6772 0.0500 0.0000 1.1589 0.0000 1.0000

3 2 4 0.0000 0.0100 3.2567 0.0000 2.0582 0.0000 1.3513

2 4 3 38.5594 11.2599 0.1898 0.0000 0.1904 0.0000 1.4041

4 3 4 63.0740 14.8127 2.9929 0.0000 0.7552 0.0000 1.3634

3 3 4 73.6721 32.6330 1.7223 0.0000 1.0221 0.0000 1.4351

3 4 3 76.5431 0.0583 0.0500 0.0000 0.4968 0.0000 2.2792 3 4 4 69.4895

5.7742 8.0001 0.0000 1.7794 0.0000 2.7889

3 5 3 88.6293 18.2614 0.8145 0.0000 -0.1780 0.0000 2.3661

2 3 5 75.0000 7.8005 0.9394 0.0000 1.3523 0.0000 1.0400

3 3 5 60.0000 40.0000 4.0000 0.0000 1.0000 0.0000 1.0400

3 2 5 0.0000 10.0000 1.0000 0.0000 1.0000 0.0000 1.0400

3 5 4 71.5444 28.1377 3.5000 0.0000 0.2169 0.0000 1.1069

5 3 5 50.6740 13.3258 0.1000 0.0000 1.0718 0.0000 1.1254

1 3 5 76.8677 5.4250 3.1105 0.0000 -0.0827 0.0000 2.1396

2 5 3 75.0000 25.0000 2.0000 0.0000 1.0000 0.0000 1.2500

3 5 5 70.0000 25.0000 2.0000 0.0000 1.0000 0.0000 1.2500

4 3 5 72.6961 30.0000 0.7795 0.0000 2.0000 0.0000 1.0500

3 4 5 76.0866 0.2500 0.1116 0.0000 0.9966 0.0000 2.5091

4 5 4 38.1011 18.9494 3.0000 0.0000 1.2274 0.0000 1.0500

4 4 5 93.0539 6.1619 1.2781 0.0000 0.5598 0.0000 1.0500

38 ! Nr of torsions;at1;at2;at3;at4;;V1;V2;V3;V2(BO);vconj;n.u;n

1 1 1 1 -0.2500 34.7453 0.0288 -6.3507 -1.6000 0.0000 0.0000

1 1 1 2 -0.2500 29.2131 0.2945 -4.9581 -2.1802 0.0000 0.0000

2 1 1 2 -0.2500 31.2081 0.4539 -4.8923 -2.2677 0.0000 0.0000

1 1 1 3 1.2799 20.7787 -0.5249 -2.5000 -1.0000 0.0000 0.0000

2 1 1 3 1.9159 19.8113 0.7914 -4.6995 -1.0000 0.0000 0.0000

3 1 1 3 -1.4477 16.6853 0.6461 -4.9622 -1.0000 0.0000 0.0000

1 1 3 1 0.4816 19.6316 -0.0057 -2.5000 -1.0000 0.0000 0.0000

1 1 3 2 1.2044 80.0000 -0.3139 -6.1481 -1.0000 0.0000 0.0000

2 1 3 1 -2.5000 31.0191 0.6165 -2.7733 -2.9807 0.0000 0.0000

2 1 3 2 -2.4875 70.8145 0.7582 -4.2274 -3.0000 0.0000 0.0000

2 1 3 3 -1.4383 80.0000 1.0000 -3.6877 -2.8000 0.0000 0.0000

3 1 3 1 -1.1390 78.0747 -0.0964 -4.5172 -3.0000 0.0000 0.0000

3 1 3 2 -2.5000 70.3345 -1.0000 -5.5315 -3.0000 0.0000 0.0000

3 1 3 3 -0.1583 20.0000 1.5000 -9.0000 -2.0000 0.0000 0.0000 1 3 3

1 0.0002 80.0000 -1.5000 -4.4848 -2.0000 0.0000 0.0000

1 3 3 2 -2.5000 0.1181 0.0268 -5.4085 -2.9498 0.0000 0.0000

2 3 3 2 0.1995 5.0000 0.2000 -2.6000 0.0000 0.0000 0.0000

1 3 3 3 0.4118 0.5219 0.9706 -2.5004 -0.9972 0.0000 0.0000

2 3 3 3 0.1000 43.1840 0.5000 -6.6539 0.0000 0.0000 0.0000

3 3 3 3 0.1000 1.0000 0.1000 -2.5000 -0.9000 0.0000 0.0000

0 1 2 0 0.0000 0.0000 0.0000 0.0000 0.0000 0.0000 0.0000

0 2 2 0 0.0000 0.0000 0.0000 0.0000 0.0000 0.0000 0.0000

0 2 3 0 0.0000 0.1000 0.0200 -2.5415 0.0000 0.0000 0.0000

0 1 1 0 0.0000 50.0000 0.3000 -4.0000 0.0000 0.0000 0.0000

0 3 3 0 0.5511 25.4150 1.1330 -5.1903 -1.0000 0.0000 0.0000

1 1 3 3 -0.0002 20.1851 0.1601 -9.0000 -2.0000 0.0000 0.0000

2 1 4 4 0.0000 0.0000 0.0000 -5.0000 0.0000 0.0000 0.0000

1 1 1 5 0.0000 19.3871 0.0103 -25.5765 -1.7255 0.0000 0.0000

5 1 1 5 0.0000 80.5586 0.1104 -8.0928 -1.7255 0.0000 0.0000

0 1 5 0 4.0000 45.8264 0.9000 -4.0000 0.0000 0.0000 0.0000

0 5 5 0 4.0000 45.8264 0.9000 -4.0000 0.0000 0.0000 0.0000

2 1 3 5 -1.5000 13.7486 0.1710 -3.7686 0.0000 0.0000 0.0000

2 3 5 3 -0.3120 -1.7990 0.2371 -3.2710 0.0000 0.0000 0.0000

1 3 5 3 -1.5000 -2.5000 0.6794 -2.5000 0.0000 0.0000 0.0000

5 3 5 3 -1.5000 7.4600 -0.9075 -9.0000 0.0000 0.0000 0.0000 2 1 5

1 0.5984 7.2907 0.1161 -5.1321 -2.1802 0.0000 0.0000 2 1 1 5 0.2704

32.0532 0.2173 -5.3228 -2.1802 0.0000 0.0000

1 1 5 1 0.5864 32.4198 -0.2514 -8.4627 -1.6000 0.0000 0.0000

1 ! Nr of hydrogen bonds;at1;at2;at3;Rhb;Dehb;vhb1

3 2 3 2.1200 -3.5800 1.4500 19.5000

The Journal of Physical Chemistry C 2019 123 (20), 12886-12893 DOI: 10.1021/acs.jpcc.9b02394

TOC Graphic